



Contents lists available at ScienceDirect



# Catalysis Today

journal homepage: [www.elsevier.com/locate/cattod](http://www.elsevier.com/locate/cattod)

## Higher alcohol synthesis over nickel-modified alkali-doped molybdenum sulfide catalysts prepared by conventional coprecipitation and coprecipitation in microemulsions

Rodrigo Suárez París<sup>a,\*</sup>, Vicente Montes<sup>b</sup>, Magali Boutonnet<sup>a</sup>, Sven Järås<sup>a</sup>

<sup>a</sup> KTH—Royal Institute of Technology, School of Chemical Science and Engineering, Department of Chemical Engineering and Technology, Stockholm, Sweden

<sup>b</sup> University of Córdoba, Organic Chemistry Department, Córdoba, Spain

### ARTICLE INFO

#### Article history:

Received 3 October 2014  
Received in revised form  
24 November 2014  
Accepted 1 December 2014  
Available online xxx

#### Keywords:

Syngas  
Higher alcohols  
 $K/MoS_2$   
Nickel  
Microemulsion

### ABSTRACT

Ethanol and higher alcohols are one of the most interesting alternatives to replace fossil fuels in the transportation sector. Nickel-modified alkali-doped molybdenum sulfide is a potential catalyst for the conversion of syngas to mixed alcohols. In this work, K-Ni-MoS<sub>2</sub> catalysts were synthesized by coprecipitation in aqueous solution or in microemulsions, followed by alkali doping. The influence of the preparation route in CO hydrogenation was investigated at 91 bar, 340/370 °C and GHSV = 2000–14,000 NmL/h g<sub>catalyst</sub>. The catalysts were also characterized by TGA, ICP, XPS, nitrogen adsorption, XRD, SEM-EDX and TEM. The novel microemulsion catalyst outperformed the conventional one, resulting in higher yields of ethanol and higher alcohols. The higher activity and selectivity was attributed to a higher concentration of promoters on the microemulsion catalyst surface, together with a lower degree of crystallinity.

© 2014 Elsevier B.V. All rights reserved.

### 1. Introduction

Environmental concerns and the shortage of fossil fuels have recently increased the search for new energy sources. Second-generation biofuels, including ethanol, are becoming a promising alternative to conventional fuels, while avoiding problems related to food and feed production [1]. Second-generation ethanol can be produced by means of either a biochemical or a thermochemical route. The thermochemical route has a higher flexibility, since a wide variety of feedstocks (e.g. lignocellulosic biomass, waste streams) can be used as raw materials to produce syngas [2]. Syngas is then catalytically converted to ethanol and higher alcohols in the so-called higher alcohol synthesis (HAS). Ethanol can be used not only as a neat fuel or fuel additive, but also as a hydrogen carrier in fuel cells [3]. Higher alcohols also have a great potential as fuel additives [4,5].

No commercial plants applying the aforementioned technology have been implemented yet, since the catalytic systems developed so far suffer from low catalytic activity, poor product distribution or severe reaction conditions [6]. Therefore, the search for a more

efficient and cheaper catalyst has become essential to make this process commercially attractive.

Although noble metal catalysts (mainly Rh-based) exhibit high ethanol selectivities, they are unattractive for commercial purposes due to the reduced availability and high cost of the metals [6]. On the other hand, non-noble catalytic systems have been widely studied and they are usually classified into three categories [3,6]: modified methanol catalysts, modified Fischer-Tropsch catalysts and modified molybdenum-based catalysts.

Molybdenum sulfide catalysts are one of the most promising options for HAS due to their sulfur resistance, high water-gas shift activity and slow deactivation by coke deposition [6,7], thus avoiding the need for ultra-desulfurization or water separation units. In addition, they are suitable for processing syngas with low H<sub>2</sub>/CO ratios, typically obtained when gasifying biomass [8]. Modification with promoters is however essential to enhance the yield of the desired products, one of the main challenges in HAS [3,6,9].

Alkali metals (Li, Na, K, Cs) have proven to shift selectivity from hydrocarbons to alcohols [6]. According to Santiesteban [10], the reaction scheme over alkali-doped molybdenum sulfide catalysts is based on a CO-insertion mechanism. The function of the alkali is to decrease the rate of hydrogenation of alkyl species and increase the rate of CO insertion [11]. Further addition of 3d transition metals (Co, Ni) increases the selectivity to ethanol and higher alcohols [3].

\* Corresponding author at: Teknikringen 42, SE-10044, Stockholm, Sweden.  
Tel.: +46 8790 8243.

E-mail address: [rosp@kth.se](mailto:rosp@kth.se) (R. Suárez París).

The microemulsion technique appears to be a suitable method to manufacture the catalyst. A microemulsion (ME) is an optically transparent and thermodynamically stable solution which consists of spherical aqueous nanodroplets stabilized by a layer of surfactant molecules [12]. Metal salts can be solubilized inside the aqueous core of the nanodroplets and then precipitated to form particles in nano-sized range and with narrow size distribution [12]. Catalysts prepared using MEs have shown enhanced properties in many applications when compared with conventional catalysts [13].

There are several studies regarding the conversion of syngas over unsupported Ni-modified K-doped molybdenum sulfide catalysts [14–18], but none of them applies the ME technique in the catalyst synthesis. The aim of this work is to develop and study the performance of a novel Ni-modified K-doped molybdenum sulfide catalyst prepared through coprecipitation in MEs and compare it with an analogous catalyst prepared by conventional coprecipitation. Two additional conventional catalysts, promoted only with nickel or potassium, have also been synthesized, characterized and tested, in order to get a better understanding of the individual effect of each promoter and be able to explain the differences between the ME catalyst and the conventional one.

## 2. Methods

### 2.1. Catalyst preparation

The bipromoted catalysts, containing both nickel and potassium, were synthesized by coprecipitation and subsequent alkali doping. The conventional catalyst was obtained through coprecipitation in aqueous solution, while the ME catalyst was obtained by mixing two water-in-oil MEs. Detailed information about the catalyst preparation procedures is shown below. The monopromoted catalysts were synthesized using the same procedure as for the conventional catalyst, but excluding the doping step with nickel ( $K\text{-MoS}_2$ ) or potassium ( $Ni\text{-MoS}_2$ ).

#### 2.1.1. Conventional catalyst

The conventional catalyst ( $K\text{-Ni-MoS}_2$ ) was prepared by adding dropwise, under continuous stirring, an aqueous solution of  $Ni(CH_3COO)_2 \cdot 4H_2O$  to an aqueous solution of  $(NH_4)_2MoS_4$ . The resulting black precipitate was aged for 24 h and then recovered by centrifugation. The recovered precipitate was first washed with deionized water (*miliQ*) and, subsequently, with a mixture of ethanol and deionized water (mass ratio 1:1). After each wash, the powder was recovered by centrifugation. The washed powder was dried at 50 °C and then crushed and sieved to a pellet size of 45–250 µm. Alkali doping was achieved by mechanically mixing the dried catalyst precursor with  $K_2CO_3$  (45–250 µm). The final catalyst was obtained after a thermal treatment at 450 °C (ramp: 20 °C/min) for 90 min, under  $H_2$  flow. A second sieving was performed to discard particles with a pellet size above 250 µm that could be formed during the heat treatment. The final sample was kept in a tightly closed container before being characterized and tested.

#### 2.1.2. Microemulsion catalyst

Two analogous water-in-oil ME systems were prepared: the first ME (ME1) contained the nickel salt and acetic acid; the second ME (ME2) contained the molybdenum salt. The detailed composition of the systems is shown in Table 1. MEs with similar composition were previously used for catalyst preparation [19–21].

The ME catalyst (ME  $K\text{-Ni-MoS}_2$ ) was prepared by adding dropwise, under continuous stirring, ME1 to ME2. The coprecipitation step is illustrated in Fig. 1. The black precipitate was aged for 24 h and then recovered by centrifugation. In order to remove surfactant and hydrocarbon residues, the washing procedure was modified:

**Table 1**  
Composition of the ME systems.

Phase	Compound (s)	Composition (wt%)
Oil	Iso-octane	53
Surfactant	CTAB	15
Co-surfactant	1-Butanol	12
Water	ME1: water, $Ni(CH_3COO)_2 \cdot 4H_2O$ , acetic acid; ME2: water, $(NH_4)_2MoS_4$	20

the precipitate was first washed with a mixture of chloroform and methanol (mass ratio 1:1) and, then, twice with methanol. The rest of the preparation procedure is analogous to that used for the conventional catalyst: drying, crushing and sieving, alkali doping and, finally, thermal decomposition under  $H_2$  flow. The temperature ramp during the  $H_2$  treatment was set to 0.5 °C/min in this case, so as to ensure complete elimination of the catalyst precursor residues not removed during the washing steps.

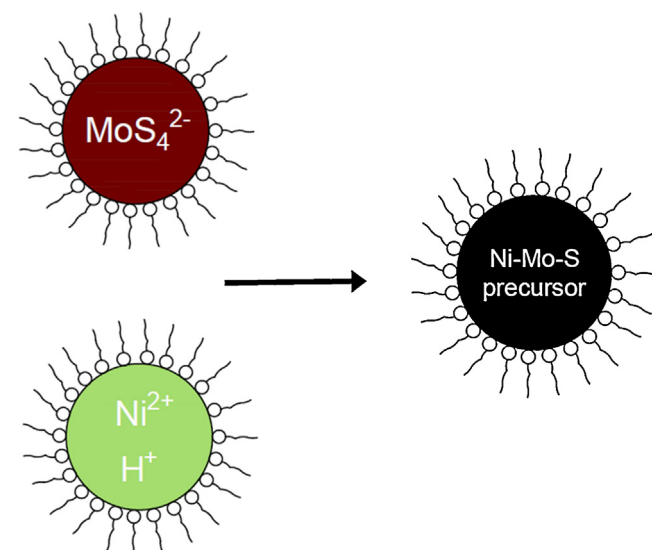
### 2.2. Catalyst characterization

A thermogravimetric analysis (TGA) of the non-calcined ME catalyst was performed on a Netzsch STA 449 F3 Jupiter instrument. The sample was subjected to the same temperature program as in the thermal decomposition (0.5 °C/min to 450 °C, held 90 min), under  $H_2$  flow. An equivalent test was also carried out on the bipromoted conventional catalyst.

The contents of nickel, potassium and molybdenum in the catalysts were determined using inductively coupled plasma-mass spectroscopy (ICP-MS), following EPA methods 200.7 and 200.8 [22,23].

X-ray photoelectron spectroscopy (XPS) data were recorded on 4 mm × 4 mm pellets, 0.5-mm thick, obtained by gently pressing the powdered materials. Prior to analysis, the pellets were outgassed in the instrument pre-chamber at 150 °C to a pressure below  $2 \times 10^{-8}$  Torr, in order to remove chemisorbed volatile species. XPS spectra were recorded on a Leibold-Heraeus LHS10 spectrometer, equipped with an EA-200MCD hemispherical electron analyzer with a dual X-ray source, using  $Mg K\alpha$  (1253.6 eV) at 120 W and 30 mA, with C(1s) as energy reference (284.6 eV).

Nitrogen adsorption measurements were performed in a Micromeritics ASAP2000 unit. The samples were outgassed by evacuation at 250 °C for a minimum of 4 h before being analyzed.

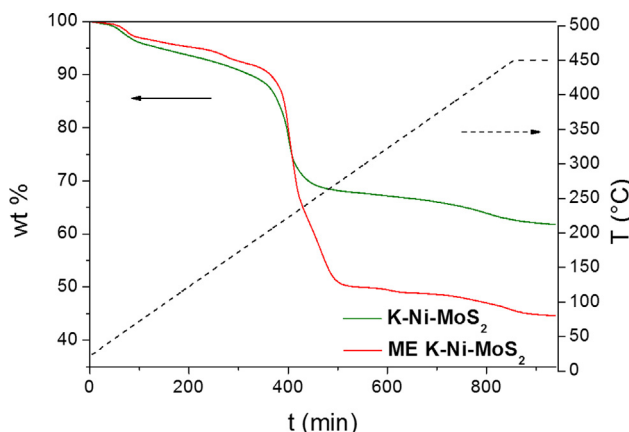


**Fig. 1.** Coprecipitation in MEs.

**Table 2**

Catalyst composition (fresh catalysts).

Catalyst	Nominal ratio (mol/mol)		ICP analysis (mol/mol)		EDX analysis (mol/mol)		XPS analysis (mol/mol)	
	Ni/Mo	K/Mo	Ni/Mo	K/Mo	Ni/Mo	K/Mo	Ni/Mo	K/Mo
K-Ni-MoS <sub>2</sub>	0.50	1.50	0.45	1.19	0.61	1.42	0.05	1.50
ME K-Ni MoS <sub>2</sub>	0.50	1.50	0.40	1.51	0.55	1.21	0.18	3.49
Ni-MoS <sub>2</sub>	0.50	0	0.50	0	0.70	0	0.14	0
K-MoS <sub>2</sub>	0	1.50	0	1.50	0	1.15	0	5.16

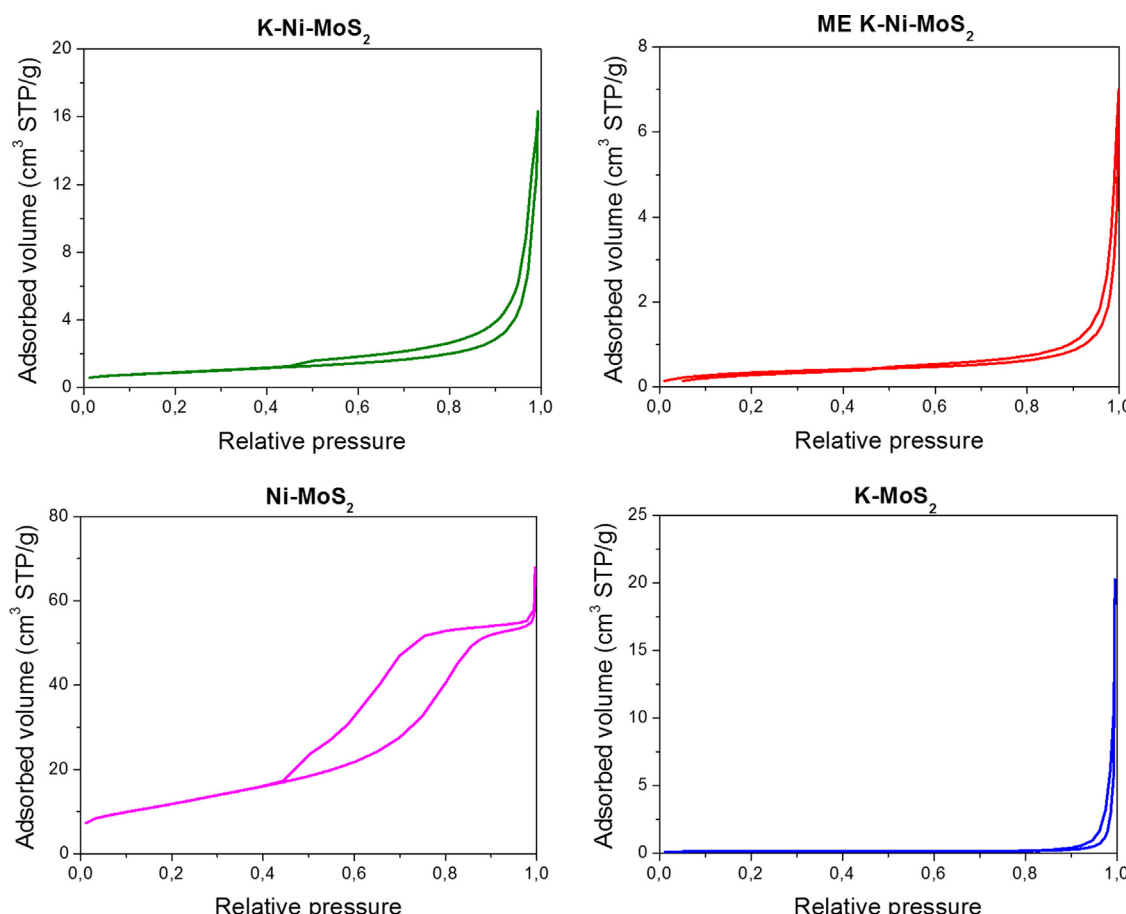
**Fig. 2.** TGA curves for the decomposition of the bipromoted catalysts.

Data were collected at liquid nitrogen boiling temperature (77 K). Surface area was calculated using the Brunauer–Emmett–Teller (BET) method with data collected at relative pressures between 0.06 and 0.2.

The patterns of X-ray diffraction (XRD) were recorded on a Siemens D5000 using Cu K $\alpha$  radiation as the X-ray source (40 kV, 30 mA). The measurements were performed at  $2\theta$  values from 5° to 60°, and at a rate of 0.12° min<sup>-1</sup>. The most probable phases in the samples were identified using the EVA software (version 13.0.0.2, 2007).

Scanning electron microscopy (SEM) images were obtained using a JEOL JSM-6300 unit equipped with an energy-dispersive X-ray (EDX) detector. It was operated at an acceleration voltage of 20 keV with a resolution of 65 eV.

Transmission electron microscopy (TEM) images were obtained using a JEOL JEM-1400 microscope. All samples were mounted on 3 mm holey carbon copper grids.

**Fig. 3.** N<sub>2</sub>-adsorption isotherms.

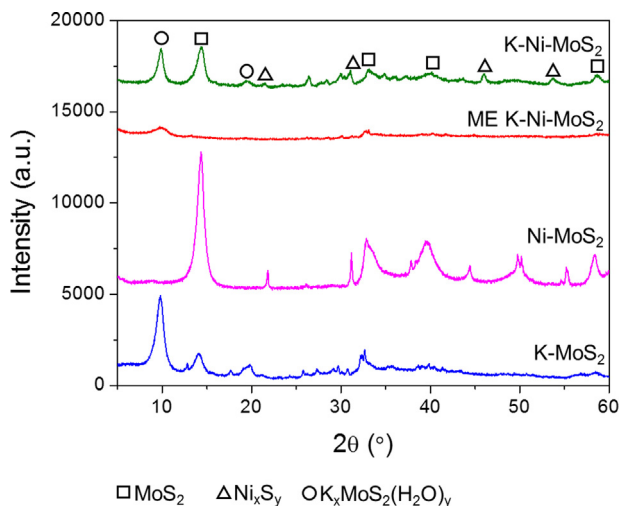


**Fig. 4.** XRD diffraction patterns.

### 2.3. Catalytic testing

CO hydrogenation reactions were performed in a high-pressure fixed-bed tubular reactor operating in down-flow mode. Approximately, 0.7 g catalyst, diluted with 3.3 g SiC (pellet size: 53–80  $\mu\text{m}$ ), were used in each test. The reactor was heated by an electric furnace and the temperature was regulated by a cascade control, with one sliding thermocouple in the catalyst bed and a second thermocouple in the oven. The dilution with SiC and this control architecture,

together with an external aluminum jacket, allowed for a temperature profile along the bed within  $\pm 0.5^\circ\text{C}$  of the set point.

A premixed syngas with  $\text{H}_2/\text{CO}$  ratio = 1 and 4%  $\text{N}_2$  as internal standard was used in the experiments. The reaction conditions were:  $P = 91$  bar,  $T = 340/370^\circ\text{C}$ . Gas hourly space velocity (GHSV) was varied between 2000 and 14,000  $\text{NmL/h g}_{\text{catalyst}}$  in order to obtain data for different conversion values. Activity and selectivity were measured on stable catalysts, after at least 100 h on stream (stabilization conditions: 91 bar, 340 °C, 6000  $\text{NmL/h g}_{\text{catalyst}}$ ). At the operating conditions used for this study, no appreciable deactivation was observed after the stabilization period, as will be shown in Section 3.

Product analysis was carried out with an on-line GC, equipped with a TCD and two FID detectors. The presented data represents the average of at least three gas composition measurements at the same reaction conditions and with carbon mass balance closures higher than 98%. More details about the reaction and analysis setup can be found in [24].

## 3. Results and discussion

### 3.1. Characterization of fresh catalysts

#### 3.1.1. Thermal decomposition

The TGA curves of the bipromoted catalysts are shown in Fig. 2. Similar patterns are obtained for both samples, with the largest weight loss occurring at temperatures between 200 and 275 °C, that is attributed to the decomposition of the precursors under  $\text{H}_2$  atmosphere. The greater decrease in the ME catalyst is due to the removal of surfactant and oil residues. As reported before for

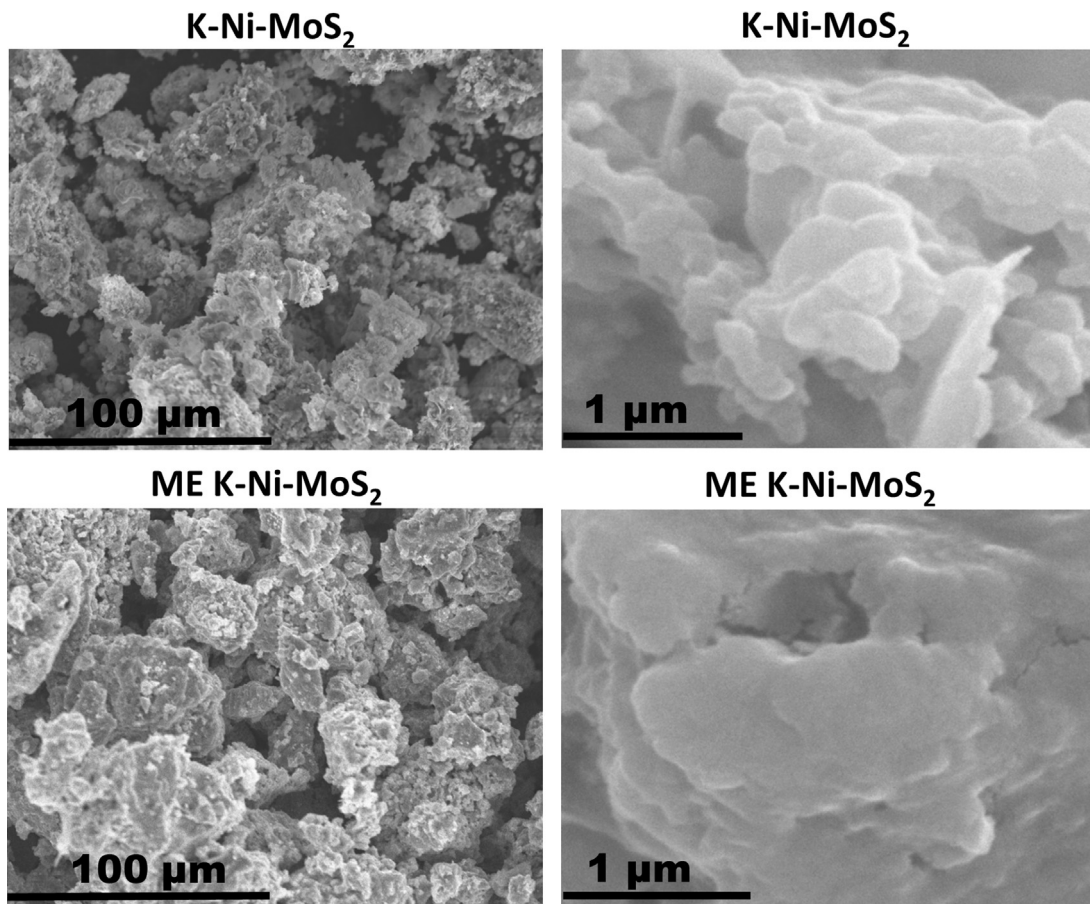


**Fig. 5.** Representative SEM micrographs of the fresh bipromoted catalysts.

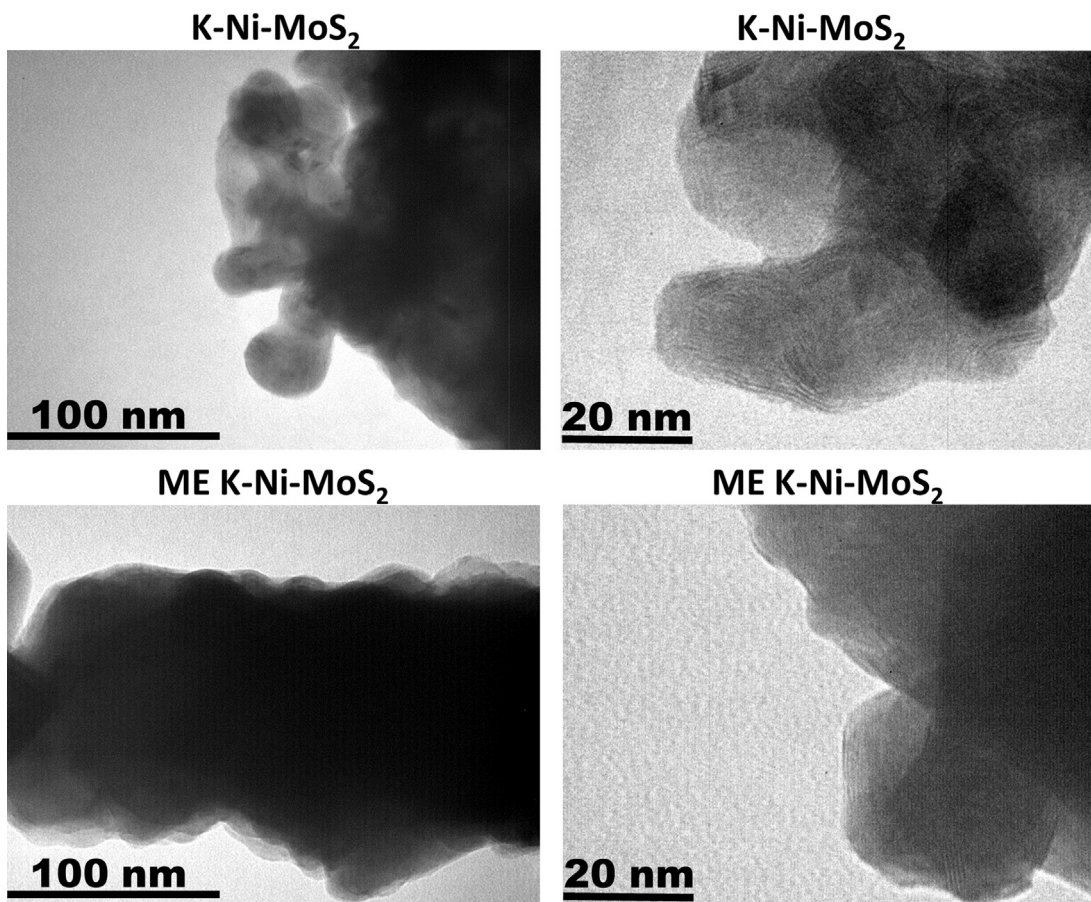


**Fig. 6.** Representative TEM micrographs of the fresh bipromoted catalysts.

analogous ME systems, there is no significant weight loss beyond 300 °C, which indicates a complete elimination of the residues [25,26].

### 3.1.2. Bulk and surface composition

The measured Ni/Mo and K/Mo molar ratios in the fresh ( $H_2$ -treated) catalysts are given in Table 2, along with the nominal ratios.

ICP and EDX analyses, which evaluate the bulk catalyst composition, show a good agreement between the nominal and the actual Ni/Mo and K/Mo ratios, with small deviations. On the other hand, XPS analyses, which give insight into the surface composition, show

greater differences among the catalysts. The higher concentration of both promoters on the surface of the ME catalyst is especially remarkable, as compared to the conventional one.

### 3.1.3. Textural characteristics

$N_2$ -adsorption isotherms for the four catalysts are shown in Fig. 3. Type II isotherms with  $H_3$ -type hysteresis loops (IUPAC classification) are observed on all the catalysts containing potassium. This behavior is characteristic of solids containing mainly macropores and consisting of aggregates or agglomerates of particles with slit-shaped pores with different sizes and shapes [27]. In contrast,

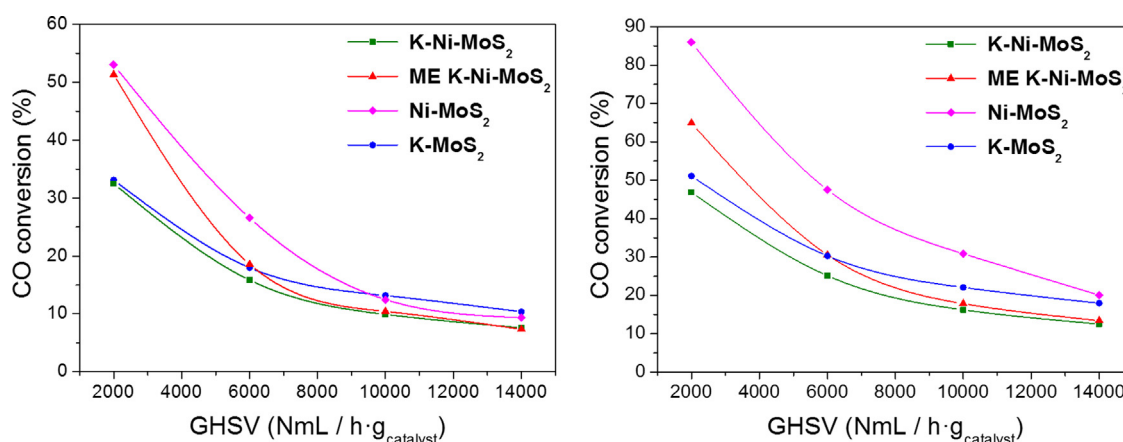


**Fig. 7.** CO conversion as a function of GHSV, at  $T = 340^\circ\text{C}$  (left) and  $T = 370^\circ\text{C}$  (right).

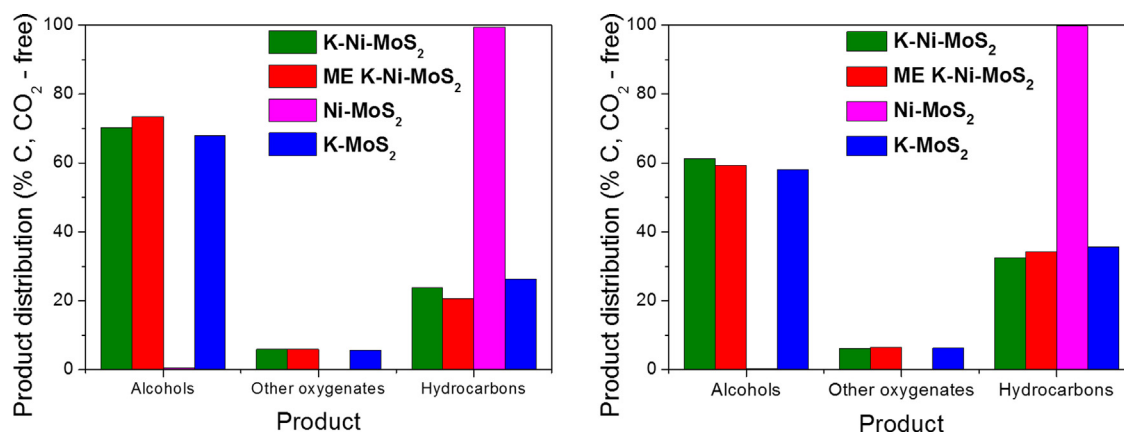


**Fig. 8.** Product distribution (GHSV = 6000 NmL/h g<sub>catalyst</sub>) at T = 340 °C (left) and T = 370 °C (right).

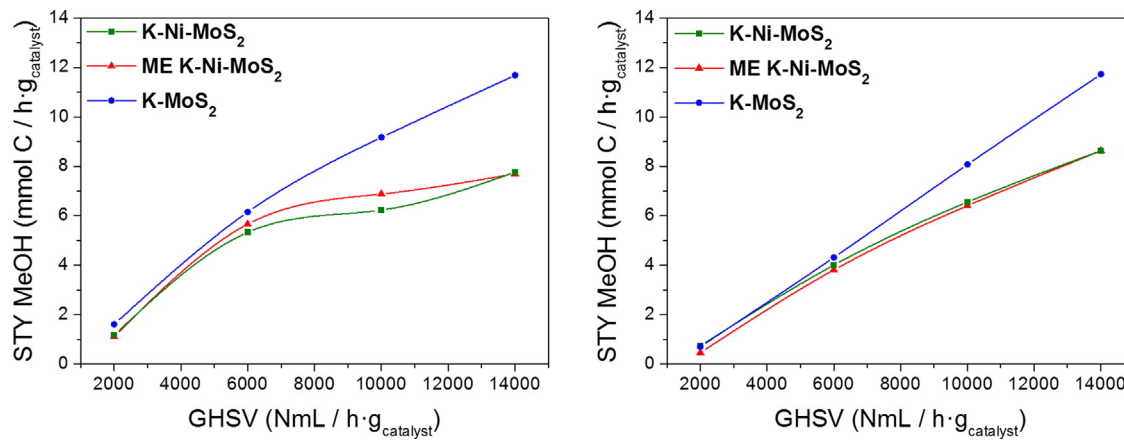


**Fig. 9.** Methanol STY as a function of GHSV, at T = 340 °C (left) and T = 370 °C (right).

Ni-MoS<sub>2</sub> exhibits a type IV isotherm, evidencing the mesoporous nature of the material [27]. It seems that potassium doping changes greatly the pore structure.

Table 3 shows the BET surface area of the catalysts, derived from the N<sub>2</sub>-adsorption measurements. Potassium doping leads to a decrease in surface area, as previously reported [14,28]. The novel ME catalyst has lower surface area than the conventional one, possibly due to the higher potassium content, detected by ICP. Even though higher surface area values have been reported for K-Ni-MoS<sub>2</sub> catalysts [15,18], the conditions used for the decomposition of ammonium tetrathiomolybdate can influence the final structure of the material and thus its surface area [29].

### 3.1.4. Bulk phase identification

The XRD diffraction patterns of the catalysts are presented in Fig. 4. Even though all the samples are amorphous to a large extent, the degree of crystallinity is especially low in the catalyst prepared with MEs, for which almost no peaks were detected.

In the conventional K-Ni-MoS<sub>2</sub> catalyst, poorly-crystallized hexagonal MoS<sub>2</sub> is identified with peaks at 2θ values of 14.4°,

33.5°, 39.5° and 58.2° [30–32]. The incorporation of nickel into the catalyst generates peaks mainly at 21.7°, 31°, 46° and 53.7°, that are attributable to the formation of Ni<sub>x</sub>S<sub>y</sub> phases [31]. Potassium doping results in two big peaks around 9.5° and 19°, which have previously been assigned to K<sub>x</sub>MoS<sub>2</sub>(H<sub>2</sub>O)<sub>y</sub>, formed due to the contact of the samples with humid air during manipulation and analysis [14]. Smaller peaks at about 30° and 31° could correspond to K<sub>2</sub>SO<sub>4</sub> [14,33] or K-Mo-S phases [18,30,34]. The superimposition and broadness of the diffraction peaks do not allow for a more comprehensive analysis.

### 3.1.5. Scanning and transmission electron microscopy

SEM micrographs do not show large morphological differences among the bipromoted catalysts. They are composed of agglomerates, showing irregular shapes with different sizes, as can be seen in Fig. 5, left. Nevertheless, higher resolution SEM images suggest

**Table 4**

Summary of operating conditions during the catalytic test.

Period (s)	Temperature (°C)	GHSV (NmL/h g <sub>catalyst</sub> )
Stabilization	340	6000
1, 5, 11	340	6000
2	340	2000
3	340	10,000
4	340	14,000
6, 10	370	6000
7	370	2000
8	370	10,000
9	370	14,000

**Table 3**

BET surface area of the catalysts as determined by N<sub>2</sub>-adsorption.

Catalyst	BET surface area (m <sup>2</sup> /g)
K-Ni-MoS <sub>2</sub>	3
ME K-Ni-MoS <sub>2</sub>	1
Ni-MoS <sub>2</sub>	43
K-MoS <sub>2</sub>	1

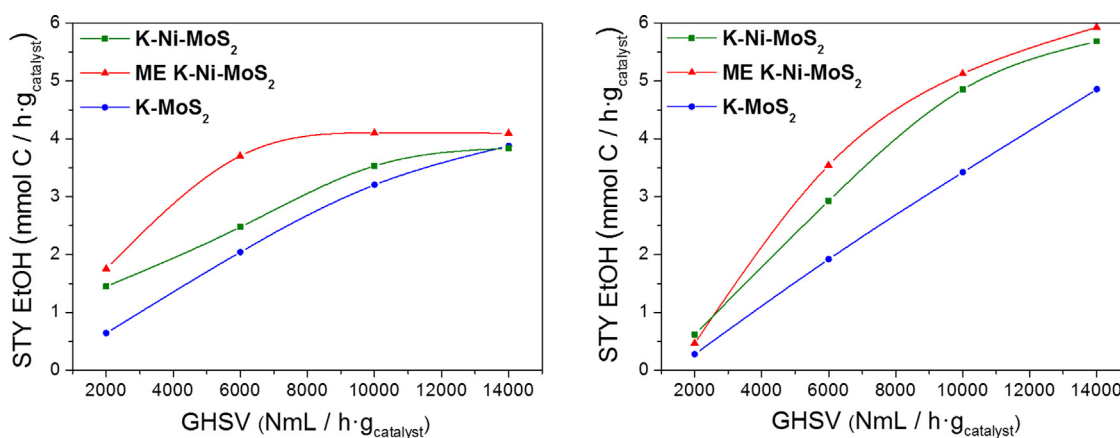


Fig. 10. Ethanol STY as a function of GHSV, at T = 340 °C (left) and T = 370 °C (right).

a lower surface area in the ME catalyst, in accordance with the N<sub>2</sub>-adsorption measurements (Fig. 5, right).

TEM micrographs (Fig. 6) show the typical layered structure of MoS<sub>2</sub>, with randomly oriented crystallites. The conventional catalyst appears to have a higher crystallinity, as already detected by XRD. Even though the resolution of the instrument did not allow for a thorough study of the nano-scale morphology, the conventional catalyst exhibits a higher stacking and length of the slabs. In contrast, the ME catalyst is composed of smaller crystallite domains. Ferrari et al. [33] have recently suggested that small crystallites may have a positive effect in the selectivity in HAS.

### 3.2. Catalytic testing: activity, selectivity and stability

CO conversion over the different catalysts at 340 and 370 °C is presented in Fig. 7. The trends are the same for both temperatures. The biggest differences appear at low space velocity values, being Ni-MoS<sub>2</sub> the most active catalyst in CO hydrogenation. However, as will be shown below, it produces mainly hydrocarbons and, therefore, it is not useful for HAS. Comparing the bipromoted samples, the novel ME catalyst shows significantly higher activity.

The product distribution (alcohols, other oxygenates, hydrocarbons) at GHSV = 6000 NmL/h g<sub>catalyst</sub> is shown in Fig. 8, indicating that potassium promotion is essential to shift the selectivity from hydrocarbons to alcohols. Promotion only with nickel is not sufficient. Nickel is a well-known methanation catalyst and Ni-MoS<sub>2</sub> yields hydrocarbons, with methane, ethane and propane comprising more than 80% of the products.

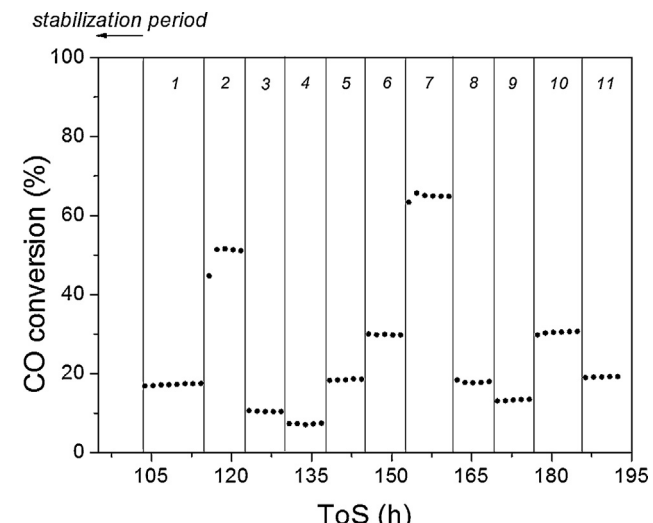


Fig. 12. CO conversion over the ME catalyst as a function of time on stream.

Figs. 9 and 10 represent methanol and ethanol space-time yields (STY) over the potassium-doped catalysts, evidencing the important effect of nickel promotion on shifting the selectivity from methanol to higher alcohols. If the bipromoted catalysts are compared, ethanol production is clearly enhanced over the ME catalyst.

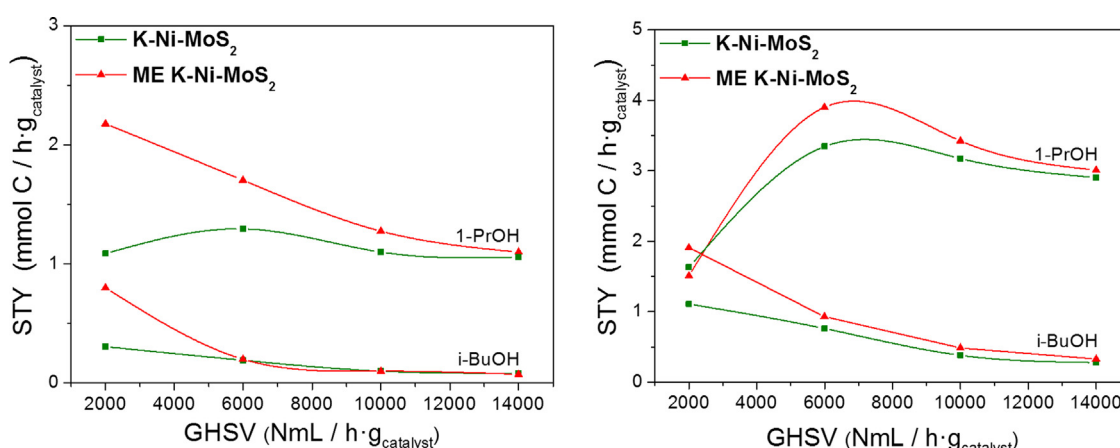
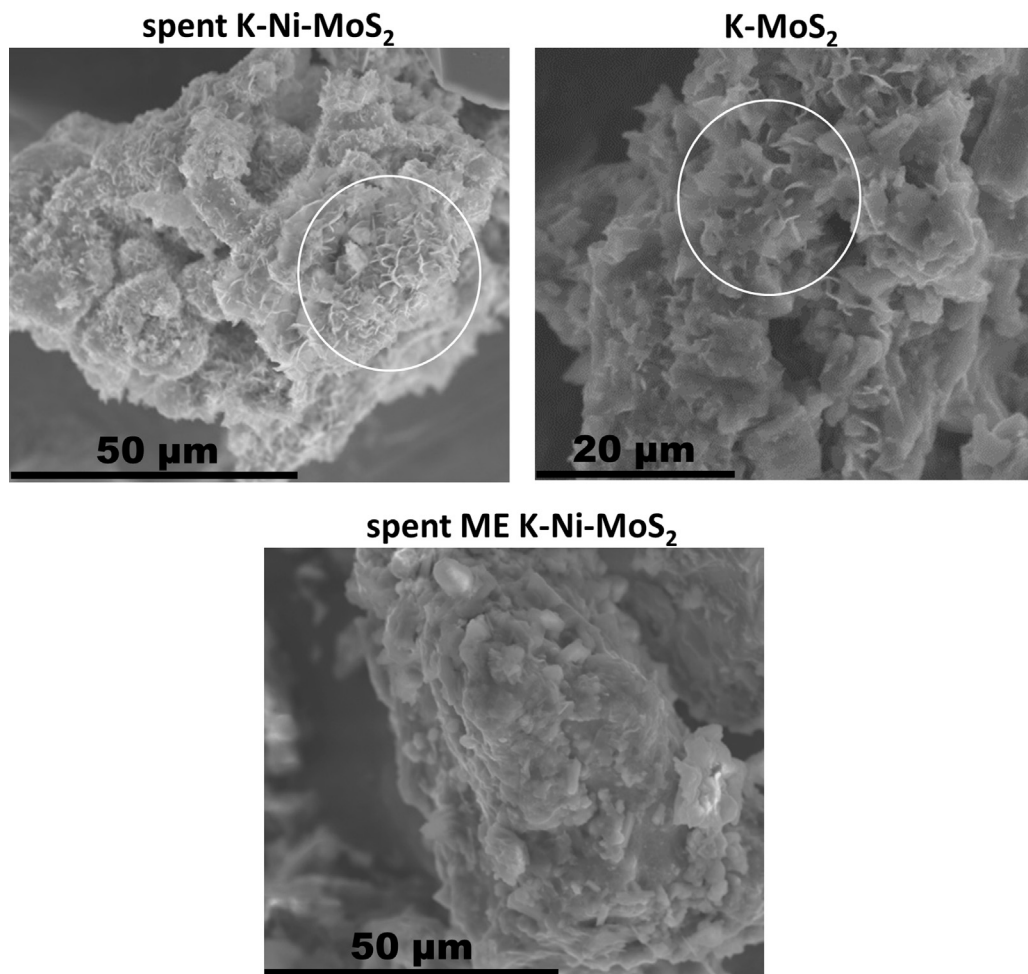


Fig. 11. 1-Propanol and iso-butanol STY as a function of GHSV, at T = 340 °C (left) and T = 370 °C (right).



**Fig. 13.** Representative SEM micrographs of the spent bipromoted catalysts.

**Table 5**

Catalytic performance of ME K-Ni-MoS<sub>2</sub> at different times on stream ( $T = 340^\circ\text{C}$ , GHSV = 6000 NmL/h g<sub>catalyst</sub>).

Time on stream (h)	CO conversion (%)	Selectivity (%C, CO <sub>2</sub> -free)					
		Methanol	Ethanol	Higher alcohols	Other oxygenates	Methane	Higher hydrocarbons
113	17.5	34.0	25.1	15.2	6.9	14.3	4.5
141	18.6	35.0	22.9	15.5	6.0	15.7	4.9
189	19.2	35.5	22.3	14.3	5.9	16.6	5.4

Concerning the alcohol distribution over the bipromoted catalysts, the most abundant high alcohols are, apart from ethanol, 1-propanol and iso-butanol. Minor amounts of other alcohols are also obtained. The ME catalyst results again in higher productivities of the aforementioned compounds, as represented in Fig. 11.

It has been reported that the selectivity on K-Ni-MoS<sub>2</sub> catalysts is very dependent on CO conversion levels [14]. Therefore, the higher selectivities to ethanol and higher alcohols over the ME catalyst could simply be attributed to the higher conversion values obtained for each space velocity, which would lead to a higher long-to-short alcohol chain ratio. However, the analysis of results at similar conversions still shows an improved performance of the ME catalyst. For example, for a CO conversion of 7.6%, the conventional catalyst results in a selectivity to ethanol and higher alcohols of 33.0% (%C, CO<sub>2</sub>-free); however, for a slightly lower conversion, 7.3%, the selectivity increases up to 35.2% (%C, CO<sub>2</sub>-free) with the novel ME catalyst. This suggests that the new preparation method does not only lead to an increase in catalyst activity but also in selectivity to the desired products. Nevertheless, the differences in selectivity

are not too big and no definitive conclusions can be drawn taking into account the small uncertainties that may be present in the measurements.

The stability of the ME catalyst has also been examined after an initial stabilization period of approximately 100 h on stream. Temperature and GHSV were modified over the following 100 h, as indicated in Table 4. No important deactivation was observed after the stabilization period, with only minor changes in activity, as shown in Fig. 12. Note that the transitions in the graph correspond to a change of the operating conditions. Examining the results at the reference conditions ( $T = 340^\circ\text{C}$ , GHSV = 6000 NmL/h g<sub>catalyst</sub>, i.e. periods 1, 5 and 11), there is a gradual increase in CO conversion, but this tendency is fairly slow (see Table 5).

In what concerns selectivity, the trends are also very slow. The selectivity values at the reference conditions have been summarized in Table 5. There is an increase in methanol and hydrocarbon selectivity, while the selectivity to the desired products (ethanol and higher alcohols) steadily decreases. Similar patterns were also

**Table 6**Catalyst composition (spent catalysts)<sup>a</sup>.

Catalyst	EDX analysis (mol/mol)		XPS analysis (mol/mol)	
	Ni/Mo	K/Mo	Ni/Mo	K/Mo
Spent K-Ni-MoS <sub>2</sub>	0.02 (0.61)	1.23 (1.42)	0.06 (0.05)	2.90 (1.50)
Spent ME K-Ni-MoS <sub>2</sub>	0.18 (0.55)	1.42 (1.21)	0.26 (0.18)	5.27 (3.49)

<sup>a</sup> The corresponding ratios in the fresh catalysts are given in brackets.

observed in the conventional sample (not shown) and have been reported before for K-Ni-MoS<sub>2</sub> catalysts [35].

### 3.3. Characterization of spent catalysts

In order to try to get a better understanding of the reasons of the improved performance of the novel ME catalyst, the spent bipromoted samples were characterized by means of EDX and XPS (Table 6). The spent samples were subjected to the same operating conditions (and similar reaction times) before being characterized: an initial stabilization period, followed by the analysis of two reaction temperatures and four different space velocities for each temperature, as summarized in Table 4.

Considering the EDX results in the fresh and spent catalysts, there is an important removal of nickel during the reaction. It is very likely due to the formation of Ni(CO)<sub>4</sub>, a compound that is thermodynamically stable under the temperature and pressure conditions within this study [36]. As a result of the formation of nickel carbonyls, nickel could be transported down the catalyst bed and, eventually, removed.

Also noteworthy is the higher concentration of nickel on the surface of the spent ME catalyst, as compared to the conventional one, a phenomenon that was also observed in the fresh catalysts. The analysis of SEM images (Fig. 13) shows a greater change in morphology, after syngas exposure, in the conventional K-Ni-MoS<sub>2</sub>, with the formation of small flakes on the surface. The same morphology is also identified in the catalyst without nickel, K-MoS<sub>2</sub>, which could be an additional indication of a higher nickel deficiency in the conventional catalyst. No appreciable morphological changes are detected in the ME catalyst.

Regarding potassium, there is a migration from the bulk to the surface of the catalysts after syngas exposure. This migration has been reported before on K-MoS<sub>2</sub> [33,37,38] and K-Co-MoS<sub>2</sub> catalysts [39,40]. DFT calculations also support the idea that potassium atoms are more energetically favored on the catalyst surface [41]. As for the nickel, the level of potassium on the surface of the spent ME catalyst is higher than on the conventional sample.

## 4. Conclusions

In this work, a novel nickel-modified potassium-doped molybdenum sulfide catalyst was synthesized through coprecipitation in microemulsion systems, characterized and tested for higher alcohol synthesis. This catalyst outperformed an analogous catalyst prepared through coprecipitation in aqueous solution.

In order to compare the performance of both catalysts, CO hydrogenation tests (H<sub>2</sub>/CO ratio = 1) were carried out at 91 bar, 340 and 370 °C, and varying the gas hourly space velocity to obtain data for different conversion levels. One important remark is the stability of the tested catalysts, since no significant deactivation was observed after an initial period of about 100 hours on stream. Activity and selectivity changes after this point were unimportant if all the operating conditions were kept constant. The microemulsion catalyst showed an improvement in both conversion and selectivity to ethanol and higher alcohols, resulting in higher yields of the desired products for the studied operating conditions.

The characterization results showed that the surface area of the microemulsion catalyst was lower. XRD patterns and TEM analysis evidenced a higher crystallinity in the conventional sample, while the microemulsion catalyst had an amorphous structure or consisted of very small crystallites. Despite a similar composition of the bulk catalysts, XPS results indicated a higher concentration of nickel and potassium on the microemulsion catalyst surface. The testing of catalysts containing only one of the promoters proved not only the importance of these elements to shift the selectivity to the desired products, but also their synergistic effect on unsupported molybdenum sulfide catalysts. Taking this into account, it is highly likely that the enrichment of nickel and potassium on the microemulsion catalyst surface is one of the main reasons for its better performance.

## Acknowledgements

KIC InnoEnergy and Junta de Andalucía (P09-FQM-4781 project) are acknowledged for the financial support. The authors are grateful to Robert Andersson and Luis Lopez (KTH) for their help in the beginning of this work. Thank you to Lina Norberg Samuelsson (KTH) for her help with the TGA analyses.

## References

- [1] R.E.H. Sims, W. Mabee, J.N. Saddler, M. Taylor, *Bioresour. Technol.* 101 (2010) 1570–1580.
- [2] G. Evans, C. Smith, in: A. Sayigh (Ed.), *Comprehensive Renewable Energy*, Elsevier, Oxford, 2012, pp. 155–204.
- [3] J.J. Spivey, A. Egbipi, *Chem. Soc. Rev.* 36 (2007) 1514–1528.
- [4] J. Campos-Fernández, J.M. Arnal, J. Gómez, M.P. Dorado, *Appl. Energy* 95 (2012) 267–275.
- [5] S. Kumar, J.H. Cho, J. Park, I. Moon, *Renew. Sustainable Energy Rev.* 22 (2013) 46–72.
- [6] V. Subramani, S.K. Gangwal, *Energy Fuels* 22 (2008) 814–839.
- [7] V.R. Surisetty, A.K. Dalai, J. Kozinski, *Appl. Catal. A: Gen.* 404 (2011) 1–11.
- [8] M.J.A. Tijmensen, A.P.C. Faaij, C.N. Hamelinck, M.R.M. van Hardeveld, *Biomass Bioenergy* 23 (2002) 129–152.
- [9] S. Zaman, K.J. Smith, *Catal. Rev. Sci. Eng.* 54 (2012) 41–132.
- [10] J.G. Santiesteban, *Alcohol Synthesis From Carbon Monoxide and Hydrogen Over Mo<sub>2</sub>-Based Catalysts*, Lehigh University, Bethlehem, PA, 1989.
- [11] X. Xiaoding, E.B.M. Doesburg, J.J.F. Scholten, *Catal. Today* 2 (1987) 125–170.
- [12] S. Eriksson, U. Nylen, S. Rojas, M. Boutonnet, *Appl. Catal. A: Gen.* 265 (2004) 207–219.
- [13] M. Boutonnet, S. Lögdberg, E. Elm Svensson, *Curr. Opin. Colloid Interface Sci.* 13 (2008) 270–286.
- [14] R. Andersson, M. Boutonnet, S. Järås, *Appl. Catal. A: Gen.* 417–418 (2012) 119–128.
- [15] D. Li, C. Yang, N. Zhao, H. Qi, W. Li, Y. Sun, B. Zhong, *Fuel Process. Technol.* 88 (2007) 125–127.
- [16] D. Li, N. Zhao, H. Qi, W. Li, Y.H. Sun, B. Zhong, *Catal. Commun.* 6 (2005) 674–678.
- [17] D.B. Li, C. Yang, H.R. Zhang, W.H. Li, Y.H. Sun, B. Zhong, in: B. Xinhe, X. Yide (Eds.), *Studies in Surface Science and Catalysis*, vol. 147, Elsevier, 2004, pp. 391–396.
- [18] H. Qi, D. Li, C. Yang, Y. Ma, W. Li, Y. Sun, B. Zhong, *Catal. Commun.* 4 (2003) 339–342.
- [19] B.J. Palla, D.O. Shah, P. Garcia-Casillas, J. Matutes-Aquino, *J. Nanoparticle Res.* 1 (1999) 215–221.
- [20] E.E. Svensson, S. Nassos, M. Boutonnet, S.G. Järås, *Catal. Today* 117 (2006) 484–490.
- [21] S. Nassos, E.E. Svensson, M. Nilsson, M. Boutonnet, S. Järås, *Appl. Catal. B: Environ.* 64 (2006) 96–102.
- [22] US EPA, Trace elements in water, solids, and biosolids by inductively coupled plasma-atomic emission spectrometry, in: *EPA Method 200.7* (revision 5.0), 2001.
- [23] US EPA, Determination of trace elements in waters and wastes by inductively coupled plasma-mass spectrometry, in: *EPA Method 200.8* (revision 5.4), 1994.
- [24] R. Andersson, M. Boutonnet, S. Järås, *J. Chromatogr. A* 1247 (2012) 134–145.
- [25] X. Liu, J. Wang, L.-M. Gan, S.-C. Ng, J. Ding, *J. Magn. Magnet. Mater.* 184 (1998) 344–354.
- [26] N. Das, R. Majumdar, A. Sen, H.S. Maiti, *Mater. Lett.* 61 (2007) 2100–2104.
- [27] G. Leofanti, M. Padovan, G. Tozzola, B. Venturelli, *Catal. Today* 41 (1998) 207–219.
- [28] T.Y. Park, I.-S. Nam, Y.G. Kim, *Ind. Eng. Chem. Res.* 36 (1997) 5246–5257.
- [29] Y. Iwata, Y. Araki, K. Honma, Y. Miki, K. Sato, H. Shimada, *Catal. Today* 65 (2001) 335–341.
- [30] V.R. Surisetty, Y. Hu, A.K. Dalai, J. Kozinski, *Appl. Catal. A: Gen.* 392 (2011) 166–172.

- [31] D. Li, C. Yang, H. Qi, H. Zhang, W. Li, Y. Sun, B. Zhong, *Catal. Commun.* 5 (2004) 605–609.
- [32] J. Irammahboob, D.O. Hill, H. Toghiani, *Appl. Surf. Sci.* 185 (2001) 72–78.
- [33] D. Ferrari, G. Budroni, L. Bisson, N.J. Rane, B.D. Dickie, J.H. Kang, S.J. Rozeveld, *Appl. Catal. A: Gen.* 462–463 (2013) 302–309.
- [34] V.R. Surisetty, A.K. Dalai, J. Kozinski, *Appl. Catal. A: Gen.* 385 (2010) 153–162.
- [35] R. Andersson, M. Boutonnet, S. Järås, *Fuel* 107 (2013) 715–723.
- [36] W.M. Shen, J.A. Dumesic, C.G. Hill Jr., *J. Catal.* 68 (1981) 152–165.
- [37] H.C. Woo, I.S. Nam, J.S. Lee, J.S. Chung, Y.G. Kim, *J. Catal.* 142 (1993) 672–690.
- [38] H. Xiao, D. Li, W. Li, Y. Sun, *Fuel Process. Technol.* 91 (2010) 383–387.
- [39] J. Irammahboob, D.O. Hill, H. Toghiani, *Appl. Catal. A: Gen.* 231 (2002) 99–108.
- [40] J. Irammahboob, H. Toghiani, D.O. Hill, *Appl. Catal. A: Gen.* 247 (2003) 207–218.
- [41] A. Andersen, S.M. Kathmann, M.A. Lilga, K.O. Albrecht, R.T. Hallen, D. Mei, *J. Phys. Chem. C* 115 (2011) 9025–9040.